Peritectic melting of mica in fault-related pseudotachylite melts and potassium mass balance as an indicator of fluid-absent source conditions.

David P. Dobson[1], Leny Montheil[2], Joseph J. Paine[1] and Andrew R. Thomson[1].

1) Department of Earth Sciences, University College London, Gower Street, London, WC1E 6BT, United Kingdom.

2) Géosciences Montpellier (UMR 5243), Université de Montpellier, PO Box 05, Montpellier 34095, France.

Abstract

Pseudotachylites are generally considered to be produced by flash melting of the most fusible minerals, with compositions often dominated by biotite mica. We present phase fraction calculations for 237 pseudotachylite analyses from 28 localities spanning a range of host rock compositions from granites to peridotites. Pseudotachylite matrix compositions cannot be reproduced by a simple linear mixture of the minerals in their host rocks and commonly show a potassium deficit in pseudotachylites which contain significant contributions from biotite or muscovite. This is strongly indicative of peritectic melting of mica under fluid-absent conditions. Occasionally, a negative contribution from an aluminosilicate phase is required but with a positive contribution from potassium feldspar. This is most consistent with peritectic melting of micas under fluid present conditions. The present data therefore suggest that, while fluid absent flash melting might be the most common mode of formation of pseudotachylite, in some instances pseudotachylites can be produced in the presence of a free fluid. Potassium mass balance of pseudotachylites might therefore be a diagnostic indicator of fluid-absent conditions in their source regions during seismogenic rupture. We give some examples of observational evidence of peritectic liquidus phases in pseudotachylites and suggest that the significance of these phases might have been overlooked in previous studies.

Key Words:

Pseudotachlyite; biotite mica; muscovite mica; dehydration melting; peritectic; liquidus phase; fluid-absent melting

Key Points:

Pseudotachylite matrix compositions cannot be reproduced by simple linear mixtures of the constituent minerals of their host rocks.

There is a potassium deficit for many pseudotachylites with a significant mica (biotite or muscovite) contribution.

This is best explained by peritectic growth of potassium feldspar during (fluid absent) dehydration melting of micas.

Introduction.

The origin of fault-hosted pseudotachylite has been the matter of some debate (Spray, 1995; Curewitz and Karson, 1999) but the current consensus is that they are produced as frictional melts during seismogenic rupture. The energy budgets of earthquake ruptures are such that, without some mitigating factor, frictional temperatures would significantly exceed the liquidus temperature of most rocks and some lubrication mechanism is required to stop wholesale melting of the deforming volume along the fault plane. Thermal pressurisation of a free fluid, where one exists, can reduce the effective normal stress (Sibson, 1975; Acosta et al., 2018; Rempel and Rice, 2006), reducing frictional heating of the rupture plane to temperatures well below the rock solidus temperature, but in fluid-absent conditions heating will progress until sufficient melt is produced to act as a lubricant (e.g.; di Toro et al., 2004). Frictional heating is rapid, resulting in flash melting of the more fusible minerals, normally micas and amphiboles, once the temperature on the rupture plane exceeds their melting temperatures (~650-850 °C for muscovite and biotite). This heating and melting process is generally thought to be so rapid that melting occurs as a closed-system process with isochemical melting of individual grains and subsequent partial reequilibration with neighbouring mineral grains by diffusion (Maddock, 1983; Lin and Shimamoto, 1998; Spray, 1992; Jiang et al., 2015).

Chemical compositions of pseudotachylites are often strongly heterogeneous, consistent with flash melting of individual grains, and also much more silica poor than their host rocks suggesting that biotite mica, in particular, often contributes disproportionately to the melt. Despite this, temperature estimates from natural pseudotachylites and experiments (see for example Dobson et al., 2018) suggest that pseudotachylites can exceed mica flash melting temperatures by several hundreds of degrees reaching 1450 °C, or more, according to some

estimates (di Toro and Pennacchioni, 2004; Caggianelli et al., 2005; Dobson et al., 2018). Pseudotachylite compositions often require a significant contribution from plagioclase melting, consistent with peak temperatures significantly exceeding the biotite and muscovite solidi and requiring diffusive reequilibration in the melt. Indeed, measurable diffusion has been shown to occur during quenching after seismogenic slip has stopped and has been used as a basis for thermal history estimates (Dobson et al., 2018).

Despite the importance of melt chemical composition in determining melting histories there have been relatively few attempts to perform mass balance calculations on pseudotachylite compositions (e.g.; Jiang et al., 2015; O'Callaghan and Osinski, 2020). Here we calculate mass balance for a compilation of published pseudotachylite compositions and demonstrate fluid-absent peritectic melting of biotite and muscovite which produces large volumes of potassium feldspar and smaller amounts of other liquidus phases as a product of the melting reaction. Closed-system melting of biotite can produce highly refractory peritectic minerals such as aluminium silicate, olivine and enstatite which will dissolve into the melt during its reequilibration with other minerals in the host rock. The occurrence of these refractory minerals in biotite melting reactions cautions against their use as indicators of very high melt temperature estimates in the absence of corroborating evidence.

Compilation of the literature.

Two hundred and thirty-seven pseudotachylite analyses from 36 studies and 28 localities were compiled from the literature, covering a range of host rock compositions ranging from highly siliceous (granite, tonalite) to highly undersaturated peridotitic compositions and including pelitic as well as igneous protoliths (Table 1). The estimated ambient conditions at the time of pseudotachylite formation ranged over 1.5 GPa > P > 10 MPa and 700 °C >T > 25 °C. Only analyses which excluded survivor clasts, described as ‘matrix’ or ‘glass’, or stated to exclude clasts were included in the compilation. Most of the compiled analyses were determined using a focussed electron microprobe beam, but some used defocussed microprobe beam, rastered microprobe beam or laser-ablation ICPMS analyses with analytical areas up to ~ 50 micrometre in size. The positions of these area analyses were such that the analyses constituted a local average of both glassy matrix and quench crystals and, hence, were believed to closely approximate the composition of the original melt. In addition, some bulk pseudotachylite analyses determined by XRF, but with survivor clast contributions

subtracted on the basis of clast volume estimates, have been included to give true average pseudotachylite compositions. There are no systematic differences between the different analysis types.

Linear Regression of Pseudotachylite Compositions.

Pseudotachylites form by frictional heating and melting of the minerals which comprise the fault gouge and wall rocks during seismogenic shear of faults. This is a complex process involving flash melting of some phases, dissolution of other phases into this initial melt, shear mixing between different melt domains and subsequent modification by quench crystallisation, devitrification and metasomatic processes. The ultimate composition of the different components (glassy matrix, quench crystals and survivor clasts) of a pseudotachylite matrix will therefore contain information about the seismogenic rupture process. Here we treat the composition of pseudotachylite matrix material (specifically, material which does not contain survivor clasts but which may or may not contain quench crystals, depending on the analytical technique and nature of the quench material) as a mixture of the minerals which melted to produce it and interpret the mixtures required to make up the pseudotachylite matrix composition in terms of melting processes and conditions. Matrix compositions, in weight percent and normalised to 100%, of pseudotachylites are calculated as linear mixtures of host-rock minerals. The eight chemical components SiO_2, TiO_2, Al_2O_3, FeO and Fe_2O_3 (calculated as FeO), CaO, MgO, Na_2O and K_2O were included in the calculation. The model concentration of the ith chemical component, C_i^m, was calculated as the sum of concentrations over n minerals, $\sum_{j=1}^{n} \varphi_j \; C_{ij}$, where φ_j is the phase fraction and C_{ij} is the concentration of component i in the jth phase. Under the constraint that the phase fractions must sum to 1, $\sum_{j=1}^{n} \varphi_j \; = 1$, the sum over all components of squared differences between the pseudotachylite concentration and the model concentration, $SS^m = \sum_{i=1}^{8} \left(C_i^{PST} - C_i^m\right)^2$, was minimised to produce the unweighted best fitting model phase fractions. The misfits were not weighted to analytical uncertainties because the uncertainties were not reported in many papers – using weighted fits where the analytical uncertainties are reported does not make a significant difference to the best fitting models. For further details of petrological mixing models see le Maitre 1982, chapter 6.

The phases used in the model included quartz, plagioclase feldspar, potassium feldspar, biotite, muscovite and ilmenite. In cases where olivine, pyroxenes, chrome spinel or hornblende were listed as being present in the host rock these were included, but minerals which were not listed were excluded from the refinement. Where mineral compositions were given these were used for the phase fitting. Where mineral compositions were not given, feldspars, micas, pyroxenes and hornblende were fitted as mixtures of end-member compositions, $NaAlSi_3O_8$, $CaAl_2Si_2O_8$, $KAlSi_3O_8$, $KMg_3AlSi_3O_{10}(OH)_2$, $KFe_3AlSi_3O_{10}(OH)_2$, $FeSiO_3$, $CaSiO_3$, $MgSiO_3$, $Ca_2(Mg_4Al)(Si_7Al)O_{22}(OH)_2$ and $Ca_2(Mg_3Al_2)(Si_6Al_2)O_{22}(OH)_2$ respectively. In these cases, the end-member mixtures were constrained by fitting a mixture model to the host rock bulk composition and the constrained end-member compositions were used for calculating the pseudotachylite mixture models. This procedure ensured that the number of independent variables, *n*-1, was equal to or less than the number of chemical components, ensuring model fits were unique. One further set of constraints was applied in constructing the mixture model such that the phase fractions for all components except for potassium feldspar were constrained to be $\varphi_j \geq 0$. Initially this constraint was also applied to potassium feldspar but it was found that many pseudotachylite concentrations could not be reasonably fitted without a negative potassium feldspar concentration, implying that potassium feldspar is created during pseudotachylite formation. On rare occasions an additional negative Al_2SiO_5 component was required to bring residual SS^m values to below 1 from values above 5 without an Al_2SiO_5 component, implying that aluminosilicate phases were also produced during pseudotachylite formation. This Al_2SiO_5 component was only added if no other combination of phases could be found which fit the data. Final best fits for tonalite and granite-hosted pseudotachylites had $1 > SS^m > 10^{-9}$and $R^2 > 0.9999$ for over 95% of analyses; the rare instances with SS^m values which could not be brought below 1 tended to be due to the model sodium-calcium ratio differing from that of the pseudotachylite sample. This is likely due to either fractional melting of feldspar, resulting in zoned plagioclase, crystallisation of feldspar microlites with a different bulk composition from the host-rock plagioclase, or inclusion of minor apatite in the bulk rock analysis which modified the apparent sodium-calcium ratio of the plagioclase determined for the rock. None of these phenomena are rare in pseudotachylites and their host rocks. Certain peridotite-hosted pseudotachylite compositions could only be fitted with mixture models containing negative olivine, diopside and chrome spinel suggesting that the pseudotachylite melt was not simply produced by

melting of the matrix minerals or that these negative phase proportion minerals were produced by the melting reaction.

Full tables of pseudotachylite compositions and their associated phase fraction model fits are given in the supplementary supporting information.

Results

Pseudotachylite model compositions, along with host-rock compositional ranges, are plotted as normalised abundances of plagioclase, mica and quartz or olivine on the triangular diagrams in figure 1. Some pseudotachylite compositions fall in the compositional fields of their host rocks but generally pseudotachylites which are found in granitic, tonalitic and sedimentary hosts show depletion in a quartz component and enrichment in a biotite component. Ultrabasic-hosted pseudotachylites show olivine-component depletion and biotite-component enrichment on this plot. The two very olivine-rich compositions are for a chrome-wehrlite host rock where the mineral assemblage used in the model did not capture the host-rock mineralogy. The olivine-rich compositions required by the model in this case are likely due to incorporation of a significant magnesium-chromite component into the melt which was not included in the model, with the extra magnesium being attributed to olivine. Pseudotachylites display strong enrichment of a mica component over their host rocks, with the exceptions of mica-free host rocks which necessarily produce melts which plot on the quartz-plagioclase or olivine-plagioclase join. This strong enrichment of mica components, and depletion in quartz component in the melt, is consistent with their relative melting temperatures as has been previously observed (Bosière, 1991; Macaudière et al., 1985) and is reflected in the relative abundance of quartz and plagioclase survivor clasts in many pseudotachylites. Some pseudotachylites hosted in granitic compositions show surprisingly high plagioclase-component concentrations. As discussed below, pseudotachylite compositions are consistently low in potassium and the high modelled plagioclase fraction might be due to a residual sodic component from the remaining alkali feldspar.

Figure 2 shows modelled feldspar components plotted against biotite components. The plagioclase-biotite plot reflects the trends discussed above, with enrichment towards biotite, and to a lesser extent towards plagioclase, relative to host rocks. The potassium feldspar-biotite plot is very different, however, with potassium feldspar ranging from 0.3 to -0.25, and negatively correlated with biotite concentration. Unlike for plagioclase there is very little

evidence of potassium feldspar-component enrichment in pseudotachylite compositions implying that there is not a significant contribution to their parent melts from melting of potassium feldspar. There is one electron microprobe spot analysis, of a sample from the Adamello tonalite, which does not follow this relationship, with a potassium feldspar phase fraction plotting off the figure, at 0.95. This sample contains significant plagioclase and K-feldspar quench microlites which might have contaminated the spot analysis of the pseudotachylite matrix.

The negative correlation between potassium feldspar and biotite components is most clearly seen in the pseudotachylites hosted in basic and ultrabasic rocks where the potassium-feldspar content of the host rocks is low (falling within the outlined blue bars in Figure 2) meaning that the melting trajectory starts from near the origin of this plot. These basic and ultrabasic-hosted pseudotachylites show two distinct trends. One group of samples extends between 0 and 0.25 biotite fraction with close to zero potassium feldspar component. The other group follows a trend which is well fitted by a linear relationship, $\varphi^{KSP} = -0.68\varphi^{BT} + 0.022$ with an R^2 value of 0.84. Pelitic and granitic-hosted pseudotachylites appear to scatter about a steeper trend than the basic-ultrabasic trend, but this is due to a significant contribution from a muscovite component which is also negatively correlated with potassium feldspar component, as shown in Figure 3. The presence of muscovite component in the mass balance also explains the four ultrabasic compositions which have zero biotite component but negative potassium feldspar component. The fit to the ultrabasic data is not significantly affected by inclusion of muscovite, with $\varphi^{KSP} = -0.64(\varphi^{BT} + \varphi^{MS}) + 0.038$ and an R^2 value of 0.71. Fits for the other host rock compositions give similar dependencies but are significantly worse due to the larger scatter of those data.

Discussion.

Causes of the negative correlation between mica and potassium feldspar.

The negative correlation between mica and potassium feldspar components in the mass balance calculations is driven by a low potassium content in the pseudotachylites. Micas and potassium feldspar are the only potassium-bearing phases in the host rocks presented here, hence there is a simple trade-off between mica and potassium feldspar components in the mass balance calculations. In cases where high mica content is required by the mass balance, for example to account for high magnesium in granite/tonalite or high aluminium in pelites,

but potassium is low, the mass balance then forces the potassium feldspar component to be negative.

While the mixing model used here can only balance a potassium deficit by having a negative potassium feldspar component, potassium depletion in pseudotachylite matrix material could be caused by three distinct processes: (1) preferential crystallisation of potassium feldspar as a quench product, (2) potassium loss during late-stage alteration, or (3) peritectic melting of mica under fluid-absent conditions.

Figure 4 shows a ternary plot of K, Al and Fe+Mg for samples recovered from seven high-speed friction experiments on granitic (Lin and Shimamoto, 1998; Montheil et al., 2020), tonalitic (Montheil et al., 2020), andesitic (Lavallée et al., 2012) and gabbroic (Lin and Shimamoto, 1998; Hirose and Shimamato, 2005) host rocks. Late-stage alteration can be ruled out for these experimental pseudotachylites and the high quenching rates of experimental pseudotachylites ensures that melts quench to pure glass. The vectors between host rock and glass compositions in this ternary plot are therefore diagnostic of the melting reactions for these samples. All samples show pseudotachylite compositions (open symbols) which either plot close to the host rock composition (solid symbols) or on vectors which aim towards the minerals that have preferentially contributed to the final melt composition. Gabbroic and andesitic samples show melting vectors which point towards the Mg+Fe or Al end members, indicative of melts dominated by either pyroxene or plagioclase respectively (see Lavallée et al., 2012 for examples of this in SEM images).

The tonalite host rock falls on the tie line between its plagioclase and biotite compositions consistent with its small modal proportion of potassium feldspar or muscovite. Pseudotachylite glasses plot towards biotite, either with a vector following the tie line as it should if it were a simple case of biotite enrichment, or with a vector which is slightly potassium depleted from the tie line. This potassium depletion requires either addition of a further Fe-Mg component, which does not exist in this rock, or crystallisation of a potassium-rich phase.

The same effect is seen in the biotite-dominated glass in granitic samples but to a much greater extent. All the granitic host rocks show some melting vectors which plot towards significant biotite-component enrichment, with all five of these biotite-melting vectors being sub parallel and plotting on the potassium-poor side of a direct vector between the host rock composition and biotite. This means that the final melt composition is depleted in potassium

relative to the best-fitting biotite content. The three most biotite-rich compositions in these granitic hosted-pseudotachylites plot in the plagioclase-biotite-pyroxene field meaning that it is impossible to produce the compositions by a simple linear mixture of the minerals in the host rock. Rather, potassium must be removed from the melt and, in these synthetic pseudotachylite samples the only mechanism available for this is crystallisation of peritectic potassium feldspar. While it is possible to produce the other two pseudotachylite compositions which plot towards biotite as a mixture of the host-rock minerals it seems more likely that they too were produced by biotite melting and peritectic potassium feldspar crystallisation since they fall on exactly the same vector as the more extremely biotite-enriched samples. If we assume that the final pseudotachylite composition is produced by a biotite peritectic reaction diluted with variable amounts of host rock composition we can calculate a biotite-potassium feldspar mass balance for the peritectic reaction. For every unit mass of biotite melted these vectors require that 0.61±0.15 units of potassium feldspar were produced, in good agreement with the trend determined from figure 2. This conclusion is further supported by thermodynamic calculations which produce peritectic feldspar for the granite-hosted pseodutachylite system of Montheil et al. (2020) (Supplementary Figure 1).

Direct observational evidence of peritectic potassium feldspar

It is reasonable to ask whether there is any direct observational evidence of peritectic potassium feldspar to back up the mass balance calculations. Synthetic samples are a useful starting point for the reasons discussed above. Backscattered electron micrographs from the granitic sample of Montheil et al (2020) show potassium feldspar overgrowths on feldspar survivor clasts with a subhedral crystal shape of the overgrowth (Figure 5a). We conclude that this overgrowth formed prior to quenching in this experiment from the following evidence; 1) the lack of any other crystalline quench phases in the glass, 2) the subhedral crystal shape which is very unlike the microlitic, spheroidal or skeletal crystal shapes typical of pseudotachylite quench material (e.g.; di Toro et al., 2004) and 3) the accumulation of small quartz survivor clasts at its margin, which implies that the overgrowth existed while the frictional melt was still shearing. Similar subhedral potassium feldspar morphologies have been seen in natural samples (Petrík et al., 2003) and as overgrowths on quartz survivor clasts.

The chemical transect in Figure 5b shows an example of a potassium feldspar overgrowing quartz in a tonalite-hosted pseudotachylite from the study of Dobson et al. (2018). The very low calcium concentration of the overgrowth is very different from the plagioclase-dominated quench microlites in this pseudotachylite, which suggests this is not a quench overgrowth and might be an example of peritectic liquidus potassium feldspar. In both of these cases the original studies were not looking for evidence of potassium feldspar growth and these features were overlooked at the time. We suggest therefore that evidence of peritectic liquidus phases, and in particular potassium feldspar, might have also been overlooked in other studies.

Peritectic melting reactions in biotite and muscovite.

Peritectic melting of biotite and muscovite to produce liquid plus potassium feldspar is well documented from fluid-undersaturated experiments (Yoder and Kushoiro, 1969; Huang and Wyllie, 1973; Brearley, 1987a; Le Breton and Thompson 1988; Pickering and Johnston, 1988) and inferred for the source of many natural migmatites under conditions of fluid-absent melting (Thompson, 1982; Clemens and Vielzeuf, 1987). In the case of melting in the presence of a free fluid the peritectic does not produce potassium feldspar as a liquidus product (Weinberg and Hasalova, 2015). The fluid-absent peritectic reaction produces further liquidus products in addition to potassium feldspar, often including a highly aluminous phase. The composition of the other phases and the mass proportions of the melting reaction depend on several factors including mica composition, pressure and temperature. Under conditions of equilibrium melting in natural metamorphic systems dehydration melting of mica also consumes other solid phases, in reactions such as:

$$6.7\ \mathrm{Msc} + 1.4\ \mathrm{Bt} + 1.4\ \mathrm{Pl} + 0.9\ \mathrm{Qtz} \rightarrow 1.0\ \mathrm{Liq} + 5.4\ \mathrm{KSp} + 1.6\ Al_2SiO_5 + 2.4\mathrm{Gt} \qquad (1),$$

for a granitic protolith at ~800 °C and 10 kbar (Pickering and Johnston, 1988). The amount of melt produced is small and the reaction products are dominated by the peritectic liquidus phases. The molar ratio of potassium feldspar to mica of 2/3 is slightly lower than the regression shown in Figure 1 which implies a molar ratio around 0.76. The reaction (1) was determined at somewhat higher pressure than the inferred conditions of formation of many pseudotachylites, and is also a eutectic rather than single-phase melting reaction, which might explain the difference in mass balance. At lower pressures, similar potassium-feldspar

producing reactions have been reported (Weinberg and Hasalova, 2015 and references therein) with an additional aluminous peritectic liquidus phase, aluminium silicate, cordierite or garnet depending on the pressure. The melting process which produces pseudotachylites differs from these metamorphic dehydration melting reactions in one important respect, namely that it is thought to be largely closed-system, single-phase, dehydration melting due to flash heating on the rupture surface (see, for example, the discussion in Bosière, 1991). The relatively few studies of closed-system dehydration melting of micas show that around 800 °C and 1 kbar biotite breaks down to a melt-bearing assemblage following the reaction (Brearley, 1987 a; b):

Bt = Liq + Fe-Al spinel + KSp +/- Al-En (2),

with similar reactions for phlogopite around 1.7 kbar and 1200 °C (Yoder and Kushoiro, 1969):

Phl = Liq+ Fo + KSp + En (3),

and muscovite at 9 kbar and 800 °C (Huang and Wyllie, 1973):

Msc = Liq + KSp + Al_2O_3 (4).

The volume of melt produced by dehydration melting of muscovite was found to be small, consistent with fact that muscovite falls close to the potassium-feldspar – corundum tie line in K-A-S-H compositional space. Potassium feldspar is not a peritectic product of melting of either biotite or muscovite under fluid saturated conditions (Huang and Wyllie, 1973; Weinberg and Hasalova, 2015), implying that, at least for cases which require negative potassium feldspar in the mass balance, pseudotachylites were produced by frictional heating of dry protolith rocks.

Other peritectic liquidus phases.

While the experimental and field studies discussed above support the current observation of potassium feldspar as a peritectic liquidus product of mica melting during seismogenic rupture, they also imply that other peritectic liquidus phases should be present in the pseudotachylites. Pseudotachylite compositions are generally well fitted ($1 > SS^m > 10^{-9}$ and $R^2 > 0.9999$) by models with either no negative phase fractions or just negative potassium feldspar. Inclusion of further phases as implied by liquidus reactions (1)-(4) can introduce redundancy to the fit causing non-unique model solutions. With the eight modelled

chemical components further peritectic liquidus products are ordinarily unresolvable, with reactions such as:

$$3Crd + 2KSp + 2H_2O = 2Bt + 6Al_2SiO_5 + 9Qtz \quad (5);$$

$$Gt + KSp + H_2O = Bt + Al_2SiO_5 + 2Qtz \quad (6);$$

$$3En + KSp + H_2O = Bt + 3Qtz \quad (7)$$

and;

$$2En = Ol + Qtz \quad (8)$$

providing redundancy for all the peritectic phases, except potassium feldspar and Al_2SiO_5, for cases where there is quartz in the protolith. In seven of our mass balance calculations, five of which also required a negative potassium feldspar component, it was necessary to include a negative contribution from Al_2SiO_5 to create compositions with high Ca and Na but low Al contents. These examples where peritectic liquidus aluminosilicate is required by the mass balance tended to be in the most extremely mica-rich compositions of pseudotachylite such as those of Petrík et al., 2003. In the case of ultrabasic protoliths, garnet and cordierite fall in the compositional null space but olivine or enstatite are required in the mass balance so their formation as peritectic products might be apparent, as is the case for some ultrabasic-hosted pseudotachylite mass balance calculations.

While not common, there is some direct observational evidence of peritectic liquidus phases in addition to potassium feldspar. The study of Clarke (1990) describes textures around relict biotites in charnokite-hosted pseudotachylites. Partially melted biotite in these samples are surrounded by coronae of sillimanite and, surrounding that, 'turbid grains' before glassy matrix material is reached. Clarke interprets the sillimanite zone as a peritectic melting product but avoids commenting on the origin of the turbid grains. Mass-balance calculations for the turbid-grains are dominated by contributions from potassium feldspar (~55%), orthopyroxene (~10%) and ilmenite (~12%) with only minor quartz (1%). Along with the sillimanite, these are likely peritectic products from reactions similar to (2) and (3) for the titanium-bearing biotite present in the charnokite host and are unlike the glassy matrix which

contains significant quartz (~18%) and plagioclase (25%). This study is quite informative since it shows that peritectic phases might not appear as large euhedral crystals and could easily be mistaken for heterogeneities in the quenched melt. It is only the careful petrography of the study, combined with the preservation of melting textures around partially-melted biotite grains which allowed the identification of peritectic phases in this case. It might therefore be that the small bright oxide particles commonly observed in biotite-dominated pseudotachylite melts represent the hercynite and magnetite peritectic liquidus products of isochemical biotite melting. Petrík et al., 2003, for example, present an image of potassium feldspar and hematite 'as products of biotite melting' without further comment.

Other refractory minerals such as mullite (Moecher and Brearley, 2004; Kirkpatrick and Rowe, 2013; Allen et al., 2002), pyroxenes and olivine (Andersen and Austrheim, 2006) have been observed and interpreted as quench crystallites, being used as evidence for very high temperatures of pseudotachylite formation (see Rowe and Griffith, 2015; Nestola et al., 2010 for further examples). However, these are also produced by some of the mica peritectic melting reactions discussed above. In the case of the ultrabasic-hosted peridotites of Corsica (Andersen and Austrheim, 2006) negative olivine, Cr-spinel and diopside are required in the mass balance and these three phases show textures (large grain sizes, equant crystal shapes, being included in quench enstatite) which suggest that they crystallised from the melt at an early stage. As discussed above, it is reasonable to expect the mass balance in these bulk compositions to show a stronger signal for the olivine and pyroxene peritectic phases than in silica-normative compositions.

It is also likely, however, that some volumetrically minor liquidus phases are consumed during subsequent reequilibration of the initial flash-melt with the other host-rock minerals as seismogenic slip progresses. This will be particularly true of olivine and pyroxenes in the granitic and tonalitic host rocks which make the bulk of the dataset, since they are not stable in the bulk composition.

Implications for pseudotachylite formation.

Of the 237 pseudotachylite analyses used in the present study 214 have significant (>1%) mica contents, 100 of which also require significant negative potassium feldspar in the mass balance. Given that many host rocks will have contained some potassium feldspar to begin

with, in which case there should be some positive contribution from potassium feldspar melting, this suggests that fluid-absent peritectic mica melting is a very common process in pseudotachylite formation. Indeed, this is the most likely explanation for the apparent lack of potassium feldspar melting in the mass balance of many granite-hosted pseudotachylites despite it having a similar (or lower) melting temperature to plagioclase which is often a major component of many pseudotachylite compositions. The present data, however, also suggest that some pseudotachylites might have formed under fluid-present conditions. The minor trend of some basic-hosted pseudotachylite samples to have substantial biotite but zero potassium feldspar components in their mass balance (figure 2) is consistent with these samples melting in the presence of a free fluid. Similarly, over half of the tonalite-hosted pseudotachylites require a positive potassium feldspar content in their mass balance calculations. In these cases, there is only a small potassium feldspar content in the host rock, so a positive value in the mass balance calculations suggests that significant amounts of peritectic potassium feldspar have not been produced. There are also two instances of pseudotachylite compositions which require negative aluminosilicate but positive potassium feldspar components. This is indicative of melting under fluid-present conditions which produces aluminoslilcate, but not potassium feldspar, as a peritectic liquidus phase. Brantut and Mitchell (2008) have shown that, if the host rock is sufficiently well drained, thermal pressurization of pore fluid can be suppressed leading to flash melting on the rupture plane even for host rocks with a free fluid. The present results are consistent with this but they suggest that fluid-free conditions might be at least as common.

Peritectic mica melting has some implications for the petrology and dynamics of formation of pseudotachylites. First, isochemical melting of muscovite, biotite and phlogopite produces highly refractory minerals (olivine, pyroxenes, aluminoslilcates and spinels) as peritectic liquidus phases at low temperatures (~800 °C for muscovite and biotite) and hence caution should be exercised in using the presence of these minerals as indicators of high melt temperatures without other corroborating evidence. Second, the mass balance of mica dehydration melting suggests that melt volumes are small. In the case of the eutectic reaction (1) the volume of melt produced is approximately 10% of the minerals consumed in the reaction, with the mass balance forming new liquidus minerals. This is likely to be an overestimate of the melt proportion produced during closed-system dehydration melting of

micas since in this case there will be no contribution to the melt from any other phases. The relatively small volumes of melt produced during flash melting of micas is unlikely to be sufficient to lubricate the sliding rupture surface. This means that shear heating will continue until either more refractory minerals reach their flash melting temperatures, or there is sufficient dissolution of the other minerals in the fault gouge into the low-volume mica melts and the system approaches a more equilibrium melt composition. This diffusive reequilibration will be enhanced by shear mixing of the melt and clasts. Finally, the processes of peritectic melting is a potential mechanism for redistributing the heat of fusion with components crystallising as overgrowths and locally releasing latent heat even as the bulk of the system is melting.

While some previous studies have observed peritectic liquidus phases resulting from biotite melting during seismogenic rupture, this is the first study to use mass-balance calculations to demonstrate just how common it is. We also note the importance of potassium mass balance as an indicator of fluid-absent conditions in the pseudotachylite source region.

Acknowledgments.

We are grateful to R Myhill and an anonymous reviewer for their insightful and positive reviews. This work was supported by the Natural Environment Research Council grants NE/M00046X/1 to DPD and NE/P017657/1 to ART.

Data availability statement.

All data are available through the citations listed in table 1.

References.

Acosta, M., Passelègue, F. X., Schubnel, A., & Violay, M. (2018). Dynamic weakening during earthquakes controlled by fluid thermodynamics. *Nature Commmmunications*, *9*, Art No 3074.

Allen, J.L., O'Hara, K.D. & Moecher, D.P. (2002). Structural geometry and thermal history of pseudotachylyte from the Homestake shear zone, Sawatch Range, Colorado. *GSA Field Guides*; *3*, 17-32. doi: 10.1130/0-8137-0003-5.17.

Altenberger, U. Prosser, G., Grande, A., Günter, C. & Langone, A. (2013). A seismogenic zone in the deep crust indicated by pseudotachylytes and ultramylonites in granulite-facies rocks of Calabria (Southern Italy). *Contrib Mineral Petrol, 166*, 975–994 DOI 10.1007/s00410-013-0904-3.

Andersen, T.B. & Austrheim, H. (2006). Fossil earthquakes recorded by pseudotachylytes in mantle peridotite from the Alpine subduction complex of Corsica. *Earth and Planetary Science Letters*, *242*, 58–72.

Boullier A.-M., Ohtani, T. Fujimoto, K. & Ito, H. (2001). Fluid inclusions in pseudotachylytes from the Nojima fault, Japan, J*. Geophys. Res*., *106*, 21,965–21,977,

Bosière, G. (1991), Petrology of pseudotachylytes from the Alpine Fault of New Zealand. *Tectonophysics*, *196*, 173-193

Brantut, N., & Mitchell, T. M. (2018). Assessing the efficiency of thermal pressurization using natural pseudotachylyte-bearing rocks. *Geophysical Research Letters*, *45*, 9533-9541. https://doi.org/10.1029/2018GL078649

Brearley, A.J. (1987). A natural example of the disequilibrium breakdown of biotite at high temperature: TEM observations and comparison with experimental kinetic data. *Mineral. Mag*., *51*, 93-106.

Brearley, A.J. (1987). An experimental and kinetic study of the breakdown of aluminous biotite at 800 °C: reaction microstructures and mineral chemistry. *Bulletin de Minéralogie*, *110*, 513-532.

Le Breton, N. & Thompson, A.B., (1988). Fluid-absent (dehydration) melting of biotite in metapelites in the early stages of crustal anatexis. *Contrib. Mineral. and Petrol*., *99*, 226–237.

Caggianelli, A., de Lorenzo, S. & Prosser, G. (2005). Modelling the heat pulses generated on a fault plane during coseismic slip: Inferences from the pseudotachylites of the Copanello cliffs (Calabria, Italy). *Tectonophysics*, *405*, 99-119.

Camacho, A. Vernon, R.H. & Fitz Gerald, J.D. (1995). Large volumes of anhydrous pseudotachylite in the Woodroffe Thrust, eastern Musgrave Ranges, Australia. *Journal of Structural Geology*, *17*, 371-383,

Clarke, G.L. (1990). Pyroxene microlites and contact metamorphism in pseudotachylite veinlets from MacRobertson Land, East Antarctica. *Australian Journal of Earth Sciences*, *37*, 1-8, DOI: 10.1080/08120099008727900.

Clemens J.D. & Vielzeuf, D. (1987). Constraints on melting and magma production in the crust. *Earth Planet. Sci. Lett*., *86*, 287-306.

Curewitz, D. & Karson, J. A. (1999). Ultracataclasis, sintering, and frictional melting in pseudotachylytes from East Greenland. *Journal of Structural Geology*, *21*, 1693-1713.

Deseta, N., Ashwal, L. D. & Anderson, T. B. (2014). Initiating intermediate-depth earthquakes: Insights from a HP–LT ophiolite from Corsica. *Lithos, 206-207*, 127-146.

Di Toro, G., & Pennacchioni, G., (2004). Superheated friction-induced melts in zoned pseudotachylytes within the Adamello tonalites (Italian Southern Alps). *Journal of Structural Geology*, *26*, 1783-1801.

Di Toro, G., Goldsby, D., & Tullis, T. E. (2004). Friction falls towards zero in quartz rock as slip velocity approaches seismic rates. *Nature*, *427*, 436–439

Dobson, D.P., Thomas, R.W. & Mitchell T.M. (2018). Diffusion profiles around quartz clasts as indicators of the thermal history of pseudotachylytes. *G-cubed*, *19*, article 16100914, doi: 10.1029/2018GC007660.

Glickson, A.Y. & Mernagh, T.P. (1990). Significance of pseudotachylite vein systems, Giles basic/ultrabasic complex, Tomkinson Ranges, western Musgrave Block, central Australia. *BMR J Australian Geol and Geophys, 11*, 509-519.

Goodwin, LB. (1999). Controls on pseudotachylyte formation during tectonic exhumation in the South Mountains metamorphic core complex, ArizonIna. in: RING,U.,BRANDON,M.T.,

LISTER,G.S,& WILLETT,S.D. (eds) Exhumation Processes: Normal Faulting, Ductile Flow and Erosion. Geological Society London, Special Publications, 1543,25-342.

Hetzel, R., Altenberger, U., & Strecker, M.R. (1996). Structural and chemical evolution of pseudotachylytes during seismic events. *Mineral. Petrol*., *58*, 33–50.

Hirose, T. & Shimamoto, T. (2005). Growth of molten zone as a mechanism of slip weakening of simulated faults in gabbro during frictional melting. *J. Geophys. Res*., *110*, B05202, doi:10.1029/2004JB003207.

Huang, W.L. & Wyllie, P.J. (1973). Melting relations of muscovite-granite to 35 kbar as a model for fusion of metamorphosed subducted oceanic sediments. *Contrib. Mineral. Petrol*., *42*, 1-14.

Jiang, H., Lee, C.-T. A., Morgan, J. K., & Ross, C. H., (2015). Geochemistry and thermodynamics of an earthquake: A case study of pseudotachylytes within mylonitic granitoid. *Earth and Planetary Science Letters*, *430*, 235-248.

Kirkpatrick, J.D. & Rowe, C.D. (2013). Disappearing ink: How pseudotachylytes are lost from the rock record. *Journal of Structural Geology*, *52*, 183-198.

Lavallée, Y. Mitchell, T.M., Heap, M.J., Vasseur, J., Hess, K.-U., Hirose, T. & Dingwell, D.B. (2012). Experimental generation of volcanic pseudotachylytes: Constraining rheology. *Journal of Structural Geology,* Volume 38, pp. 222-233.

Le Maitre, R.W. (1982). *Developments in Petrology*, Volume 8. Numerical Petrology: Statistical Interpretation of Geochemical Data. Elsevier, 281 pp.

Lin, A., (1994). Glassy pseudotachylyte veins from the Fuyun fault zone, northwest China. *Journal of Structural Geology, 16*, pp. 71-83.

Lin, A., (2008). Seismic Slip in the Lower Crust Inferred from Granulite-related Pseudotachylyte in the Woodroffe Thrust, Central Australia. *Pure and Applied Geophysics, 165*, 215-233.

Lin, A., & Shimamoto, T., (1998) Selective melting processes as inferred from experimentally generated pseudotachylytes. *J. Asian Earth Sci*., *16*, 533–545.

Lin, A., Sun, Z. & Yang, Z., (2003). Multiple generations of pseudotachylyte in the brittle to ductile regimes, Qinling–Dabie Shan ultrahigh-pressure metamorphic complex, central China. *The Island Arc*, *12*, 423-435.

Lund, M. G. & Austrheim, H. (2003). High-pressure metamorphism and deep-crustal seismicity: evidence from contemporaneous formation of pseudotachylytes and eclogite facies coronas. *Tectonophysics, 372*, 59-83.

Macaudière, J., Brown, W.L. & Ohnenstetter, D., (1985). Microcrystalline textures resulting from rapid crystallization in a pseudotachylyte melt in a meta-anorthosite. *Contrib. Mineral. Petrol*., *89*, 39-51.

Maddock, R. H. (1983). Melt origin of fault-generated pseudotachylytes demonstrated by textures. *Geology, 11*, 105-108.

Magloughlin, J.F., (1989). The nature and significance of pseudotachylyte from the Nason terrane, North Cascade Mountains, Washington. *Journal of Structural Geology, 11*, 907-917.

Magloughlin, J. F., (1992). Microstructural and chemical changes associated with cataclasis and frictional melting at shallow crustal levels: the cataclasite-pseudotachylyte connection. *Tectonophysics, 204*, 243-260.

Mahapatro, S.N., Tripathy, A.K., Nanda, J.K. & Roy, A. (2009). Coexisting ultramylonite and pseudotachylyte from the eastern segment of the Mahanadi shear zone, Eastern Ghats Mobile Belt. *J Geol Soc India*, *74*, 679-689.

Moecher, D.P. & Brearley, A.J. (2004). Mineralogy and petrology of a mullite- bearing pseudotachylyte: Constraints on the temperature of coseismic frictional fusion. *American Mineralogist*, *89*, 1486–1495.

Montheil L., Toy, V.G., Scott J.M., Mitchell T.M. and Dobson D.P. (2020). Impact of coseismic frictional melting on particle size, shape distribution and chemistry of experimentally-

generated pseudotachylite: examples from tonalite and Westerly Granite Submitted to: *Frontiers in Earth Science*.

Nestola, F., Mittempergher, S., Di Toro, G., Zorzi F. & Pedron, D. (2010). Evidence of dmisteinbergite (hexagonal form of CaAl2Si2O8) in pseudotachylyte: A tool to constrain the thermal history of a seismic event. *American Mineralogist, 95*, 405–409.

O'Callaghan, J. W. & Osinski, G. R. (2020). Geochemical and petrographic variations in pseudotachylyte along the Outer Hebrides Fault Zone, Scotland. *Journal of the Geological Society, 177*, 50–65.

Patro, R., Mahapatro, S. N., Bhattacharya, A., Pant, N. C., Nanda, J. K., Dey, A., & Tripathy, A. K. (2011). Chemical heterogeneity in an enderbite- hosted pseudotachylite, eastern India: Evidence for syn-deformation multi-reaction melting in pseudotachylite. *Contributions to Mineralogy and Petrology*, *161*, 547–563. https://doi.org/10.1007/s00410-010-0548-5

Petrík, I. Nabelek, P.I. Janaák, M. & Plašenka, D. (2003). Conditions of Formation and Crystallization Kinetics of Highly Oxidized Pseudotachylytes from the High Tatras (Slovakia) *J.Petrol*., *44*, 901-927.

Pickering, J.M. & Johnston, D.A. (1988). Fluid-absent melting behaviour of a two-mica metapelite: experimental constraints on the origin of Black Hills granite. *J.Pet*., *39*, 1787–1804.

Plattner, U., Markl, G. & Sherlock, S (2003). Chemical heterogeneities of Caledonian (?) pseudotachylites in the Eidsfjord Anorthosite, North Norway. *Contrib Mineral Petrol, 145*, 316-338.

Rempel, A., & Rice, J. R. (2006). Thermal pressurization and onset of melting in fault zones. *Journal of Geophysical Research*, *111*, B09314.

Ritchie, S.D. (2009). Alpine Fault Pseudotachylites. Thesis, U. Ontago

Rowe, C.D. & Griffith, W.A. (2015). Do faults preserve a record of seismic slip: A second opinion. *J. Struct. Geol*., *78*, 1-26. doi.: 10.1016/j.jsg.2015.06.006

Sibson, R. H. (1975). Generation of Pseudotachylyte by Ancient Seismic Faulting. *Geophysical Journal International*, *43*, 775-794.

Spray, J. G. (1987). Artificial generation of pseudotachylyte using friction welding apparatus: simulation of melting on a fault plane. *Journal of Structural Geology*, *9*, 49-60.

Spray, J.G., (1992). A physical basis for the frictional melting of some rock-forming minerals. *Tectonophysics, 204*, 205–221.

Spray, J.G., (1995). Pseudotachylyte controversy: fact or friction? *Geology, 23*, 1119–1122.

Thompson, A.B. (1982). Dehydration melting of pelitic rocks and the generation of H20-undersaturated granitic liquids. *Am. J. Sci*., *282*, 1567-159.

Toyoshima, T. (1990). Pseudotachylyte from the Main Zone of the Hidaka metamorphic belt, Hokkaido, northern Japan. *Metamorphic Geology, 8*, 507-523.

Ujiie, K., Haruka, Y., Sakaguchi, A. & Toh, S. (2007). Pseudotachylytes in an ancient accretionary complex and implications for melt lubrication during subduction zone earthquakes. *Journal of Structural Geology, 29,* 599-613.

Ujiie, K., Tsutsumi, A., Fialko, Y. & Yamaguchi, H. (2009). Experimental investigation of frictional melting of argillite at high slip rates: Implications for seismic slip in subduction-accretion complexes. *J. Geophys. Res., 114*, B04308, doi:10.1029/2008JB006165.

Yoder, H. S. & Kushiro, I. (1969). Melting of a hydrous phase: phlogopite. *Am. J. Sci*., *267A*, 558–582.

Warr, L., & van de Pluijm, B. (2005). Crystal fractionation in the friction melts of seismic faults (Alpine Fault, New Zealand) *Tectonophysics, 402*, 111-124.

Weinberg, R.F. & Hasalova, P. (2015). Water-fluxed melting of the continental crust: A review. *Lithos*, *212–215*, 158–188.

Figure Captions

Figure 1. Triangular plots of normalized quartz-mica-plagioclase and olivine-mica-plagioclase content of pseudotachylites. Host rock compositional ranges are indicated. Abbreviations GR, TO, SED and B-UB denote granitic, tonalitic, sedimentary and basic-ultrabasic protoliths respectively. Grey fields mark the range of host rocks..

Figure 2. Model phase fractions of biotite versus (a) plagioclase feldspar and (b) potassium feldspar. The depletion in quartz and enrichment in biotite in pseudotachylites compared to their host rocks is clear. Potassium-feldspar shows a negative correlation with biotite content, extending in negative phase fractions. The solid line is the best first-order polynomial fit to the basic-ultrabasic suite..

Figure 3. Triangular diagram of normalised phase fractions of biotite, muscovite and potassium-feldspar. Negative model phase fractions of potassium-feldspar are projected from the biotite –muscovite tie line using the potassium feldspar apex as the projection focal point.

Figure 4. Triangular diagram of Mg+Fe-Al-K, in weight percent, for synthetic pseudotachylites and their host rocks for granitic, tonalitic and gabbroic samples. Open symbols are for pseudotachylite glass compositions and solid symbols are for host rock compositions. Arrows show vectors from rock compositions to the pseudotachylite compositions which they host. Granite-hosted pseudotachylites which plot a long way from their host-rock compositions plot on vectors which can only be produced by biotite melting with peritectic potassium-feldspar. Mineral compositions are marked in black.

Figure 5. Two examples of potassium feldspar growing from pseudotachylite melt. (A) A subhedral crystal of potassium feldspar showing overgrowth texture and small quartz clasts accumulating at its edges, from the granite-hosted sample studied by Montheil et al., 2020. (B) Chemical transect from a quartz survivor clast into the quenched melt showing a potassium feldspar rim. The horizontal dashed lines show the Si, Al and K composition of end-member potassium feldspar. From the tonalite-hosted sample studied by Dobson et al., 2018.

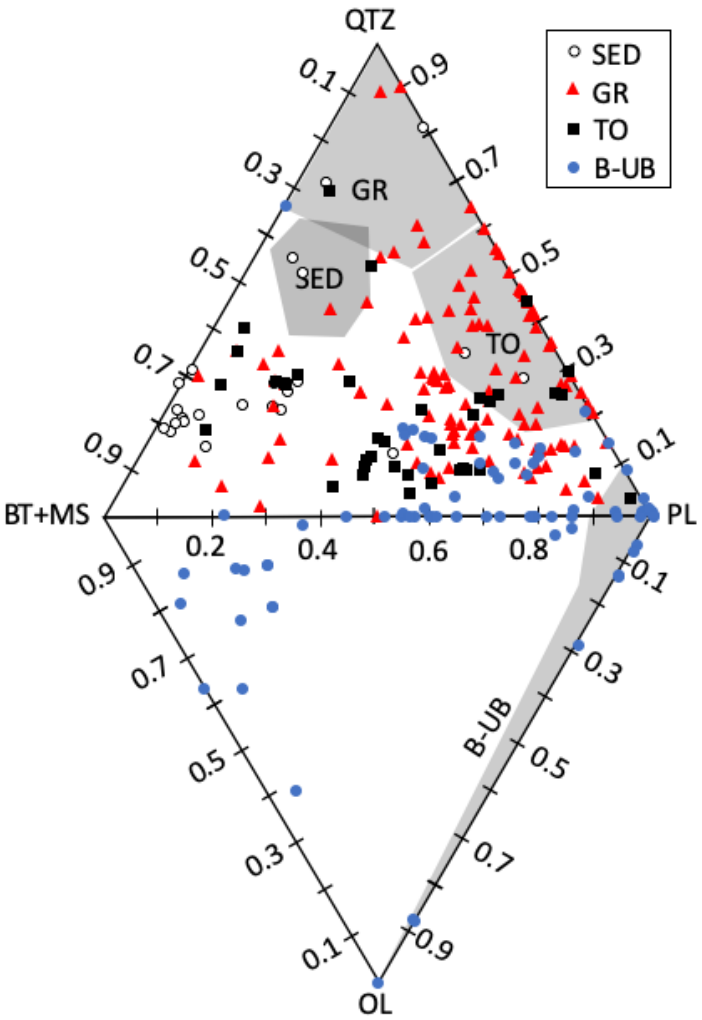

Figure 1

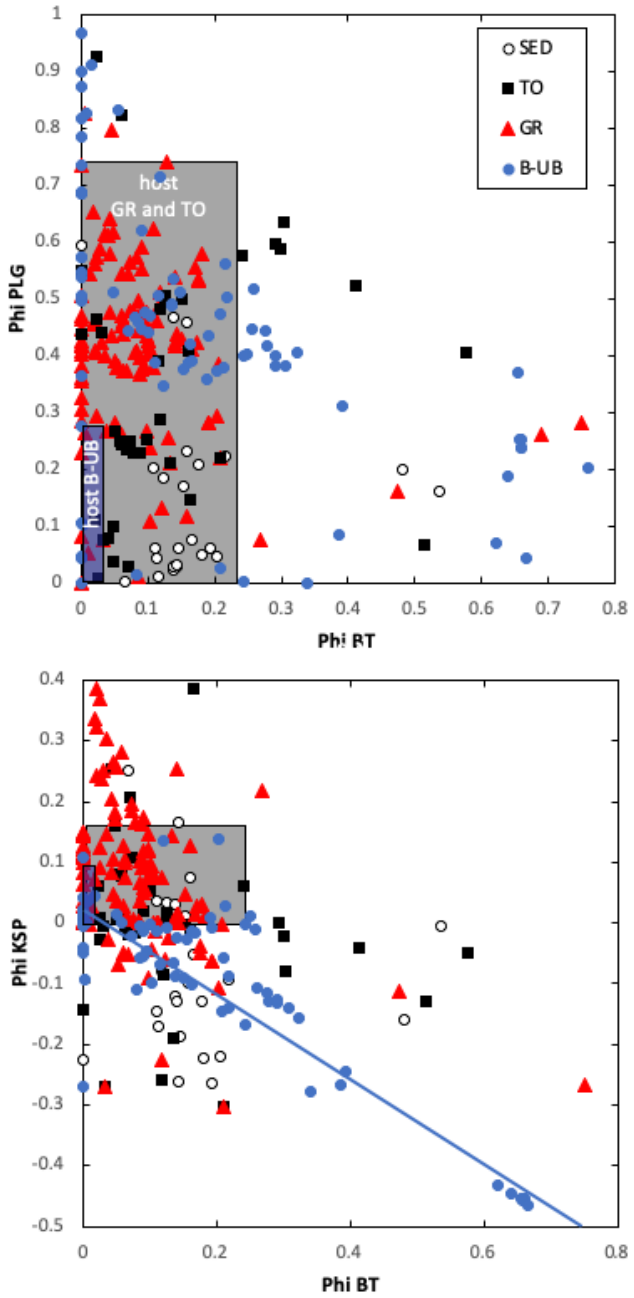
SED
TO
GR
B-UB
host
GR and TO
host B-UB
Phi PLG
Phi BT
Phi KSP
Phi BT

Figure 2.

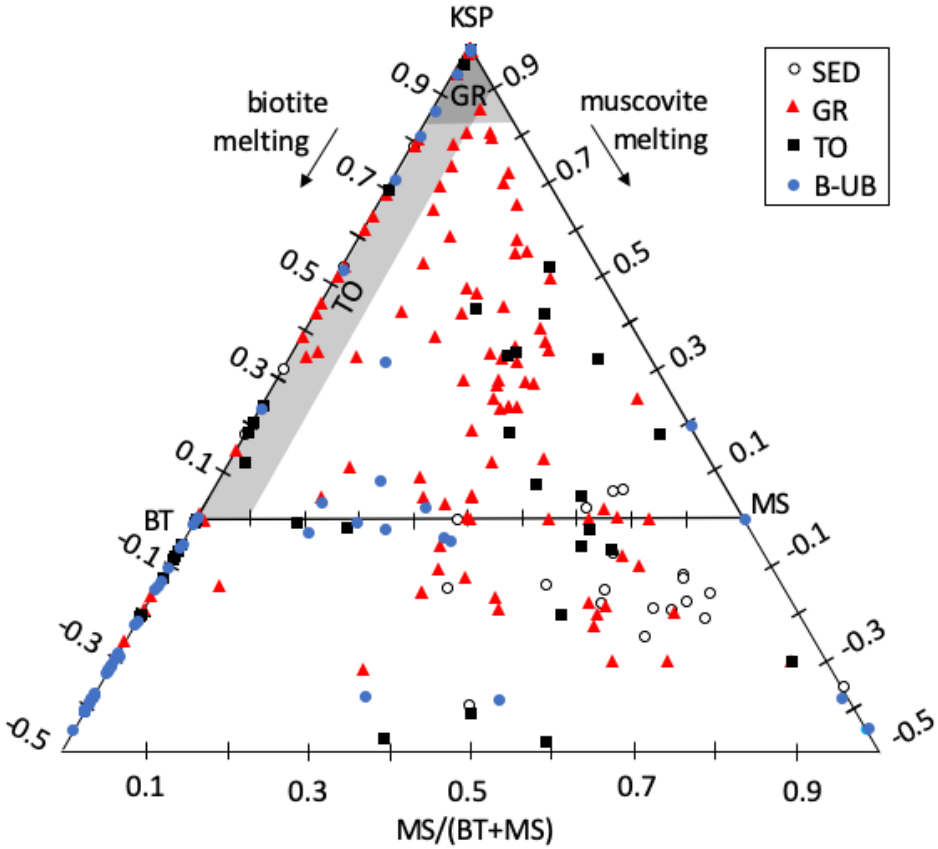
KSP
biotite
melting
muscovite
melting
SED
GR
TO
B-UB
BT
MS
0.9
0.7
0.5
0.3
0.1
-0.1
-0.3
-0.5
0.1
0.3
0.5
0.7
0.9
MS/(BT+MS)

Figure 3.

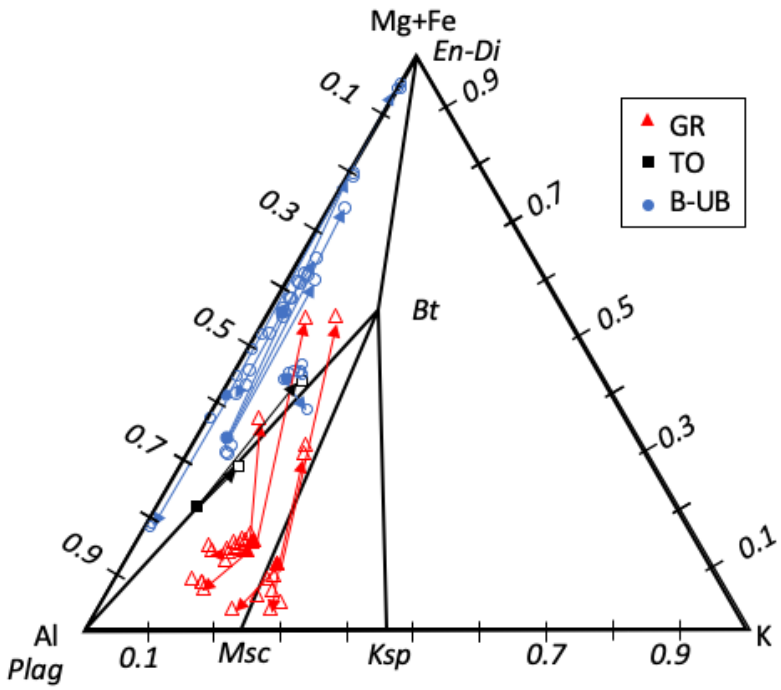
Mg+Fe
En-Di
0.1
0.3
0.5
0.7
0.9
0.9
0.7
0.5
0.3
0.1
GR
TO
B-UB
Bt
Al
Plag
0.1
Msc
Ksp
0.7
0.9
K

Figure 4.

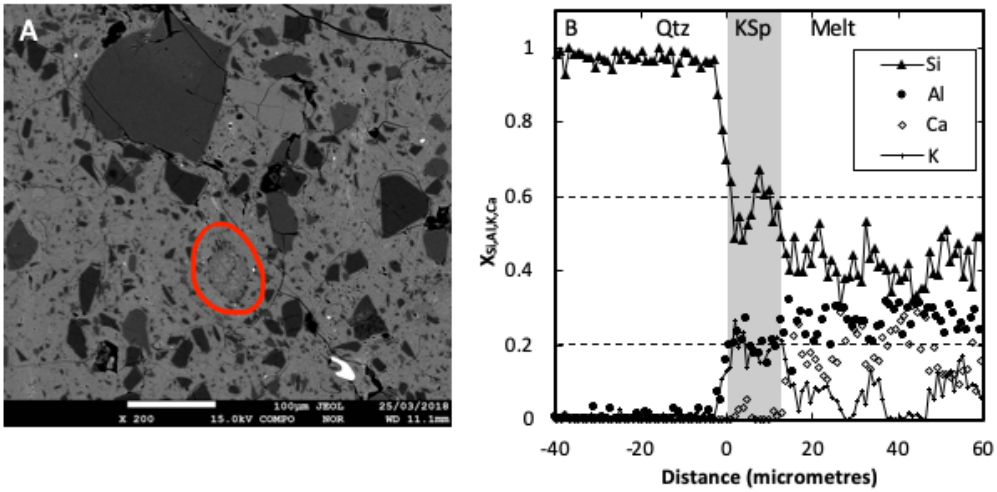
A
B
Qtz
KSp
Melt
Si
Al
Ca
K
$X_{Si,Al,K,Ca}$
Distance (micrometres)
1
0.8
0.6
0.4
0.2
0
-40
-20
0
20
40
60

Figure 5.